JCTC Journal of Chemical Theory and Computation

pubs.acs.org/JCTC Article

A Strategy for Modeling Nonstatistical Reactivity Effects: Combining Chemical Activation Estimates with a Vibrational Relaxation Model

Tomislav Rožić, Matthew S. Teynor, Nađa Došlić, David M. Leitner, and Gemma C. Solomon*

Cite This: J. Chem. Theory Comput. 2024, 20, 9048−9059 Read Online

ABSTRACT: The kinetics of many chemical reactions can be readily explained with a statistical approach, for example, using a form of transition state theory and comparing calculated Gibbs energies along the reaction coordinate(s). However, there are cases where this approach fails, notably when the vibrational relaxation of the molecule to its statistical equilibrium occurs on the same time scale as the reaction dynamics, whether it is caused by slow relaxation, a fast reaction, or both. These nonstatistical phenomena are then often explored computationally using (quasi)classical ab initio molecular dynamics by calculating a large number of trajectories while being prone to issues such as zero-point energy leakage. On the other side of the field, we see resource-intensive quantum dynamics simulations, which significantly limit the size of explorable systems. We find that using a Fermi's golden rule type of model for vibrational relaxation, based on anharmonic coupling constants, we can extract the same qualitative information while giving insights into how to enhance (or destroy) the bottlenecks causing the phenomena. We present this model as a middle ground for exploring complex nonstatistical behavior, capable of treating medium-sized organic molecules or biologically relevant fragments. We also cover the challenges involved, in particular quantifying the excess energy in terms of vibrational modes. Relying on readily available electronic structure methods and providing results in a simple master equation form, this model shows promise as a screening tool for opportunities in mode-selective chemistry without external control.

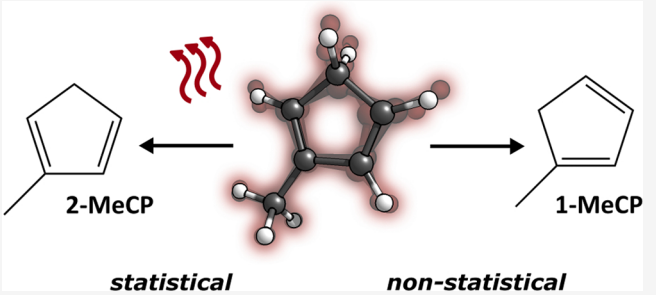

INTRODUCTION

Nonstatistical reactivity has grown to become a broad term in the literature that describes chemical systems undergoing dynamics that do not conform to the well-established statistical transition state theory (TST). Transition state theory, also known as the activated complex theory, was developed in the 1930s with ideal gas reactions in mind and has since seen widespread use in efficiently computing reaction rates.[1] The simplest forms of TST, taught in chemical thermodynamics courses and used throughout computational organic chemistry is based on the Eyring-Polanyi equation:

$$k = \frac{\kappa k_B T}{h} e^{-\Delta G^{\ddagger}/RT} \quad (1)$$

To calculate the reaction rate k one only needs to provide the temperature of the system and estimate the Gibbs energy of activation, $\Delta G^{\ddagger}$. The transmission coefficient κ accounts for how often the system recrosses the transition state and is often assumed to be 1. The standard TST calculation will also simplify away from the Gibbs energy and express this equation via the (adiabatic) reaction barrier ΔV.[2]

The simplicity of these models is quite powerful, as it reduces the problem to comparing only the energies of single points of the multidimensional potential energy surface (PES) − minima for reactants, products, or intermediates and first-order saddle points for transition states (TS). Once these points are located, an additional calculation can be performed to obtain the entropic correction required for Gibbs energies. Many quantum chemistry software packages also provide relatively "black box" methods that aid in the search for transition states.

Further developments of this theory include, among others: defining a surface in the PES called a diving surface (variational TST)[3] or better describing the transition state region by redefining a classical Hamiltonian at the TS geometry (semiclassical TST).[2] An approach that goes hand in hand with these theories is predicting product ratios of chemical reactions based on the relative computed energies of the major products. This can also be done with Rice−Ramsperger−Kassel−Marcus (RRKM) theory, which is more suitable than

Received: August 2, 2024
Revised: September 19, 2024
Accepted: September 25, 2024
Published: October 2, 2024

standard TST for reactions that do not reach thermal equilibrium.

Nonstatistical Reactivity. When this statistical approach to reactivity fails, the reaction scheme could be incomplete or not modeled rigorously enough (or both). In a publication by Glowacki et al.[4] we see an informative example of the former, as a seemingly complex enzyme reaction is made simple again once the authors include just one more conformer to their statistical model. Therefore, we need to be careful not to mislabel reactions in which there are other competing mechanisms present.

In this work, we choose to focus on nonstatistical effects caused by the complex dynamics of the reacting molecule(s). Simply put, these effects can be attributed to overlapping time scales, usually assumed to be separate. For example, during a chemical reaction, the system can find itself vibrationally excited. The excess energy could originate from a molecular collision, the absorption of a photon or it could be left over from a previous reaction step (for instance, a bond forming or breaking). In those cases, the molecule is often termed chemically activated and labeled in reaction schemes with a *.

If vibrational relaxation is slow (or the reaction occurs very quickly) the system does not reach a thermal equilibrium that can be described statistically (thermalize) before the reaction moves forward and the two processes cannot be separated. A cartoon example is shown in Figure 1, though if we were drawing an accurate PES, the excess energy would also place the reaction dynamics "higher" above the path, which in turn makes the landscape (local minima and barriers) less restrictive. In other words, the separate reaction steps cannot be considered as a Markov chain as a system that does not thermalize in time is not completely "memoryless". This goes against the main assumptions of TST, where the activated complex is in thermal equilibrium and its vibrations are populated according to the Boltzmann distribution, as well as RRKM where such coupling is not included.

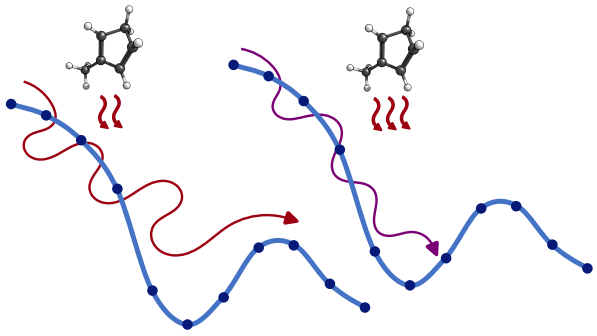

Figure 1. While it is hard to visualize in one dimension, it helps to remember most vibrations are oscillations from the proposed reaction path. Higher levels of excitation correspond to larger oscillations and higher reactivity if there are other minima nearby to explore. If the drop down the PES is steep enough and relaxation slow (as shown on the left example), some parts of it could be hopped over, including nearby barriers. In that case, molecular vibrations are underdamped. As relaxation becomes faster, it is as if the molecule moves on the PES with more friction (right).

The vibrational energy/population of a molecule can then influence the reaction and result in experimental product ratios significantly different from TST predictions.[5] In reactions facilitated by collisions, reactivity can be enhanced by reactant and product vibrational modes matching the reaction coordinate.[6] In extreme cases, one can find reactions that seem to proceed "uphill" on the PES.[7] Sometimes intermediates that would be relevant steps for TST could end up being less explored, or even skipped completely in cases of "ballistic" movement.[8] We could even think of these effects as an extreme case of kinetic versus thermodynamic reaction control, presenting at the scale of a single molecule.

A very common approach to model chemical reactivity (both statistical and nonstatistical) is to sample a larger part of the Born−Oppenheimer PES with ab initio classical molecular dynamics (AIMD).[9] The chemical system is propagated classically, using Newton's laws of motion for the nuclei, though the forces that act on them are computed through quantum mechanics (QM), or if that is too resource-intensive, with predefined force fields. Another alternative is to propagate an atom-centered density matrix. Conclusions are then drawn from a number of trajectories containing information about the position and velocity of the nuclei over time.[9−14]

Looking for these dynamic effects in the literature can be demanding as they are often described independently in different research fields. Along with examples cited above, we point out two very descriptive terms: dynamic matching,[15] implying some molecules are filtered through a preceding transition state and already possess dynamics matched to the reaction coordinate, and flyby reaction trajectories[16] where extrinsic force enables skipping certain side reactions. A perspective on dynamic effects in organic chemistry, including those not caused by vibrationally hot molecules, can be found in ref 17.

All these topics touch upon localized energy or directional movement on the PES. However, intramolecular vibrational energy redistribution (IVR) itself is also directional and energy does not move equally from one vibrational mode to another.[18,19] The simplest way to put it is that not all degrees of freedom will be equal when it comes to exchanging energy, and up to a certain time scale the energy can at the same time be distributed unevenly and also flow in predetermined directions. There are also doubts about using AIMD trajectories for vibrational relaxation modeling due to a lack of correspondence with actual quantum dynamics such as the issue of zero-point energy leakage. For further reading, we refer to a recent chemical perspective on IVR modeling in ref 20.

Furthermore, dynamic effects can be present even if the separation of time scales required for applying TST is present. For example, relaxation can be faster than the overall reaction rate, yet still slower than the barrier crossing, resulting in a reduced reaction rate ($\kappa < 1$ in eq 1). For a broader review of vibrational energy flow and its effects on chemical reactivity, we suggest reading the review in ref 21, which includes the well-studied examples of cyclohexane ring inversion in solution and stilbene photoisomerization in molecular beams and gas phase, reaching high-density gases.

Substitutions that do not change the overall mechanism could then lead to some amount of control over the selectivity of desired products.[22] In a recent work by Chen et al., different pathways to the same products can result in different vibrational populations and affect subsequent reaction steps, potentially allowing for reaction control at more than one point by exciting or modifying the vibrational modes involved.[23]

This concept has led to plenty of research over the years in the hope of mastering mode-specific laser-driven chemistry,

https://doi.org/10.1021/acs.jctc.4c01011
J. Chem. Theory Comput. 2024, 20, 9048−9059

where reactions can be tailored and guided by pumping energy into certain vibrational modes, for instance using an infrared laser pulse to climb the vibrational ladder[24] until dissociation occurs and "quantum control"[25] strategies in general. Recently, the field saw a surge of activity in modifying reactivity by coupling molecular vibrational modes with an optical cavity, termed polariton chemistry.[26,27] In this approach, the cavity in which the reaction takes place is tailored for an interaction with a vibrational mode such that it fortuitously influences the reaction.

If it is not probable we can deposit energy in all the right places, for example with lasers, we wish to use the overall direction of vibrational energy flow to guide the chemical excitation we already have available to useful regions of the molecular system. Or in case of fortuitous "mode-matching" present from the start, we wish to keep it localized for longer. Constructing a special environment, such as an optical cavity, will not always be viable if several modes need to be coupled simultaneously or the reaction conditions do not allow it.

Therefore, we propose an efficient methodology that aims to predict how tuning the molecular structure of a system changes this vibrational scaffolding while still preserving the overall reaction mechanism.

THE WORKFLOW

In this work, we propose a workflow that combines estimating the vibrational excitation of the reacting system with a vibrational relaxation model that relies on (third-order) anharmonic coupling constants to describe the structure-based directionality of IVR and identify key relaxation pathways.

In the first half of the article, we will walk through the process (and obstacles) of obtaining all the required data through an example of a known nonstatistical chemical reaction, after which we will introduce the IVR model itself in detail and the conclusions we draw from it. An overview of the procedure discussed in this article is given in Figure 2.

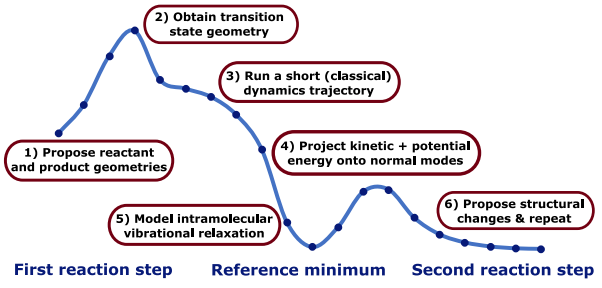

Figure 2. A summary of the modeling scheme required to explore a two-step reaction. In the background: energy profile of the first and second step of the example reaction (for cyclopentadiene) obtained with NEB-CI at the BS UCAM-B3LYP+D3BJ/def2-TZVP level of theory. Note that computing the reaction path is not required if the TS is easily obtained.

We will consider a common theme in nonstatistical reactions: a reaction with several steps in which the first step releases a relatively large amount of energy. We assume that at each subsequent reaction step, there is an excess of energy (compared to thermal equilibrium) stored in molecular vibrations. We will choose the first "activated" product (or intermediate) as our reference, which means we will use its vibrational normal modes when describing energy localization. The question is then whether the energy stays long enough in the reactive mode(s) that match the next step of the reaction, or if the energy dissipates quickly to the rest of the molecule—and the solvent. In this context, the reactive mode(s) could also be those enabling some yield-decreasing side reaction. Whether these modes are populated right away or depend on IVR to reach them would depend on the energy released during the previous step.

Our example reaction, shown in Scheme 1, is a ring-breaking reaction followed by a rearrangement. The rearranged product,

Scheme 1. Reaction Scheme for the Ring Opening of 2-MeBCP[a]

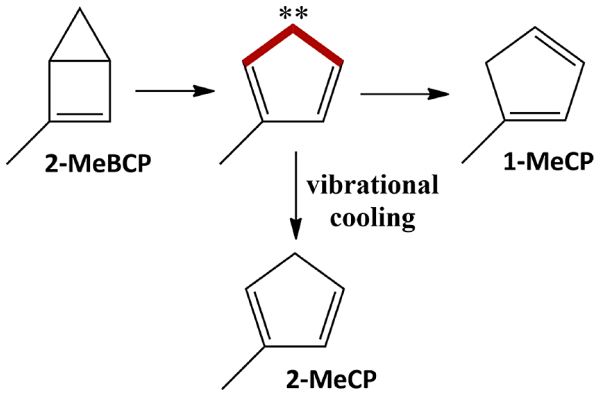

[a]After the initial ring opening, the vibrationally excited product (affected atoms highlighted in red) can undergo a further rearrangement, a process which, according to ref 31, competes with the collisional cooling of the initial product.

1-methylcyclopentadiene (**1-MeCP**), is observed in larger quantities than expected compared to the initial product, **2-MeCP**. The rearrangement is reported to occur on the same time scale as the vibrational relaxation of the molecule[28] and the surprising product ratio is therefore attributed to the nonstatistical dynamics the initial product undergoes while it is still chemically activated.

While the mechanism of the ring opening of bicyclo[2.1.0]-pent-2-ene(s) has attracted a fair amount of attention,[28−30] the main reason we chose this reaction is that it is computationally nontrivial and explored in the more recent work by Goldman et al.[31] In the article they model a reduced system (without the methyl group) using nearly two thousand AIMD trajectories at very high temperatures of 1000−2000 K and at the BS-UO3LYP/3-21G level of theory.

Excitation Estimation. Since we are dealing with a reaction and not a laser experiment, the first piece of the puzzle is quantifying what being "chemically activated" means in this context. We assume that the activation lies in excess vibrational energy right after the bond breaking. We then choose to stay in the frame of reference of the initially formed product, **2-MeCP**, by using its calculated vibrational normal modes and coupling constants for the vibrational relaxation model.

The first step is to estimate where this excess energy is located, that is how much of it is initially deposited in the populations of each of the product's vibrational normal modes.

We see three ways of approaching this problem, of which we will explore the first two:

https://doi.org/10.1021/acs.jctc.4c01011
J. Chem. Theory Comput. 2024, 20, 9048−9059

1. Run a shorter AIMD simulation from the TS geometry and decompose the resulting geometry and kinetic energy of the nuclei within the normal mode picture. The work by Goldman et al.[31] does this, using bond lengths as stopping criteria.
2. Compare key geometries along the reaction path (such as the TS) in terms of displacements along the normal modes and using only these displacements as estimates of vibrational excitation.
3. "Eye-ball" one or several modes that best match the proposed reaction step (or use a computed intrinsic reaction coordinate) and inspect their decay separately. This is the simplest approach but puts us at risk of missing out on information that is not as visually obvious (for example, bond stretching as a result of the bond order changing).

In all three cases, a reasonable transition state geometry is useful (or mandatory). For this purpose, we locate the transition state (**TS**) between the original two-ring structure (**2-MeBCP**) and the first product (**2-MeCP**).

We utilize the climbing image variant of the nudged elastic band method (NEB-CI)[32] as implemented in ORCA[33] for a relatively black-box approach to obtaining both the minimum energy path (MEP) of the reaction and potential transition states and intermediates along that path. After a converged NEB-CI calculation, a TS optimization is performed at the same level of theory. The result can be seen in Figure 3.

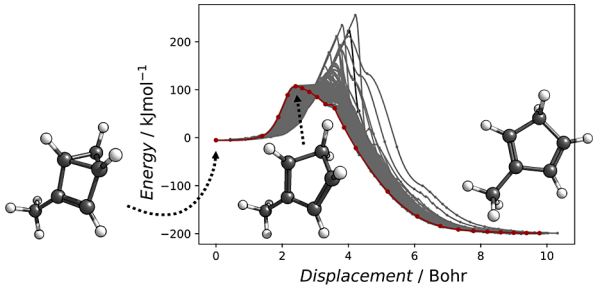

Figure 3. Final minimal energy path (red) for the MeCP ring-opening reaction with only the initial (left) and final (right) molecular geometries given as inputs. The converged MEP provides a transition state guess (middle) that is only 3 subsequent optimization steps from a converged TS geometry. In the background, in gray, are the previous iterations.

Additionally, we perform an NEB calculation between the TS and the second product, **1-MeCP** to gauge barrier sizes (see Figure S2 for discussion). In short, the 100 kJ mol^{-1} (24 kcal mol^{-1}) barrier between the two products is not easily overcome at room temperature but is roughly a third of the energy released during the ring opening.

At this point, we should warn that dealing with reactions where bonds break can lead to areas along the proposed reaction path where the molecule is not well-defined with a single-reference electronic structure method. In our case, singlet diradical character is present, from a configuration where the ring-forming single bond has been broken, but the electrons have not yet rearranged to form new double bonds. Our transition state geometry lies exactly in this area, something that can be quantified with the T_1 diagnostic (see Figure S3).

This failure of the chosen electronic structure method would also, at least in our experience, cause failure to converge the NEB-CI path. We find, however, that using an unrestricted formalism of DFT we obtain reasonable MEPs. All that needs to be done to confirm the proposed TS is to perform a subsequent geometry optimization and frequency calculation using a broken-symmetry approach at the same level of theory.

This success is not surprising as broken-symmetry unrestricted DFT with a hybrid functional has been shown to provide an adequate description of organic molecules with diradical character, including transition states,[13,34,35] polarizabilities[36] and bond breaking in general.[37,38] In the work by Hamaguchi et al.,[39] we see an example of a reaction both involving diradicals and dynamic effects modeled with unrestricted DFT. As we are interested in geometries and not precise energies, we see no need to apply additional spin projection correction schemes. We do note a warning from ref 40. that discrepancies in calculated broken-symmetry geometries could be larger when dealing with systems where the radical character is very delocalized (for example, due to π conjugation). With these warnings in mind, we consider the potential discrepancies to be small enough for our use case.

This detour still keeps our approach relatively black-box, as only simple keywords for the SCF procedure (such as "brokensym 1,1" in ORCA or "guess = mix" in Gaussian) are required to obtain a broken-symmetry wave function solution. Now that we have obtained a transition state geometry, we will address the first two proposed ways of quantifying the vibrational excitation of a "hot" molecule.

In the normal mode picture of approach (ii), we stay in the frame of reference of the **2-MeCP** product. The difference between this minimum geometry and the TS geometry is then expressed in terms of dimensionless normal coordinates. First, the two geometries are optimally aligned according to the Kabsch algorithm. The differences in the positions of each atom are then projected onto the normal modes of the product to obtain the dimensionless mode displacements Q. A detailed look at the procedure can be found in the SI. The potential energy is then estimated as

$$V_\alpha = \frac{\omega_\alpha^2 Q_\alpha^2}{2} \tag{2}$$

This assignment is a common approach in spectroscopy, for example when mapping the PES between the initial Franck–Condon (vertical) excitation and a nearby conical intersection[41] or to estimate rearrangement energy in electron transfer calculations.[42] Since it is based on the harmonic approximation, the approach will fail if the geometries are too different and/or if the reaction coordinate is very anharmonic.

An example of this can be seen in Figure 4, which shows an AIMD trajectory of the system, starting at the transition state geometry. At the first point, the projection onto normal modes (red) estimates an unrealistically high potential energy compared to the relative electronic energy obtained by BS DFT. This would result in a large overestimation of the initial energy present in the vibrational modes. However, in case all the energies are overestimated similarly, the results would not change. For this reason, we will not immediately discard approach (ii).

Since the relatively affordable broken-symmetry DFT calculation provides a good estimate of the barrier height, we are encouraged to move on to approach (i) and perform an AIMD simulation. The goal now is to determine whether a single "drop" down the PES, which we choose to term a "0 K

https://doi.org/10.1021/acs.jctc.4c01011
J. Chem. Theory Comput. 2024, 20, 9048−9059

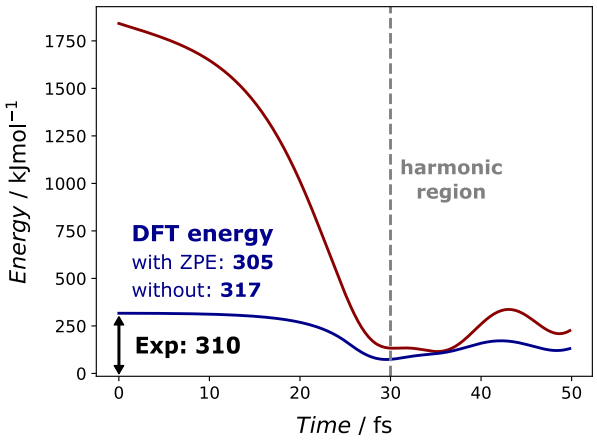

Figure 4. Figure shows a comparison of the computed electronic energy (dark blue) and the sum of the estimated energies from the harmonic projection scheme (dark red) with reference to the **CP** minimum during a "0 K pushed" trajectory started at the **BCP** transition state. The gray dotted line points out the chosen time step, at which the system is in the harmonic basin near its minimum, though it does not pass directly over it. If the discrepancy in energies is too large, the trajectory needs to be rejected.

pushed trajectory", provides similar results to a much more costly ensemble sampled at the experimental temperature of 303 K. The 0 K pushed trajectory will start without any additional energy (not even zero point energy) other than 0.5 kcal mol^{-1} (around 2 kJ mol^{-1}) in the imaginary, reaction-driving mode.

This slight "push" saves some computational time and ensures the correct direction of the trajectory. For our purpose we will aim to run the trajectories just long enough for the molecule to "drop" down into the harmonic area of the PES to quantify which modes of the product end up vibrationally excited in the process. In short, we are performing the same projection based on normal mode displacements, but closer to where it is theoretically sound to do so.

The appropriate point in all trajectories can be determined automatically. We chose to look for points at which the sum of the calculated electronic and projected potential energies is the smallest. This ensures picking a trajectory step that is near the minimum, where the potential energy projection is more accurate. Ideally, this would be the point closest to the minimum before its first "bounce", even if the trajectory approaches closer later on. The energy profile of an example trajectory is shown in Figure 4. Note that despite "bouncing" quite high up the PES, this trajectory is not reactive and either unmanageably long simulations or unphysically high temperatures would be required to directly sample the next reaction step.

Both the projections of the kinetic and potential energies onto the normal modes are then used as the initial energies for the time evolution of a more simplified vibrational relaxation model.

Modeling Intramolecular Vibrational Relaxation. The IVR model we use (eqs 3 and 4) originates from phonon scattering theory[43] and estimates the flow of excess vibrational energy Γ from mode α into two other modes (represented by β and γ), depending on how well they match in frequencies ω (that is, energy), their mean Bose−Einstein occupation numbers n and their third order anharmonic coupling constant $\Phi_{\alpha\beta\gamma}$.

$$\Gamma_{\alpha}^{\text{decay}} = \frac{\hbar}{16\omega_{\alpha}} \sum_{\beta,\gamma} \frac{|\Phi_{\alpha\beta\gamma}|^2 (1 + n_{\beta} + n_{\gamma})}{\omega_{\beta}\omega_{\gamma}} \times \frac{(\Gamma_{\alpha} + \Gamma_{\beta} + \Gamma_{\gamma})}{(\omega_{\alpha} - \omega_{\beta} - \omega_{\gamma})^2 + \frac{1}{4}(\Gamma_{\alpha} + \Gamma_{\beta} + \Gamma_{\gamma})^2} \quad (3)$$

$$\Gamma_{\alpha}^{\text{collision}} = \frac{\hbar}{8\omega_{\alpha}} \sum_{\beta,\gamma} \frac{|\Phi_{\alpha\beta\gamma}|^2 (n_{\beta} - n_{\gamma})}{\omega_{\beta}\omega_{\gamma}} \times \frac{(\Gamma_{\alpha} + \Gamma_{\beta} + \Gamma_{\gamma})}{(\omega_{\alpha} + \omega_{\beta} - \omega_{\gamma})^2 + \frac{1}{4}(\Gamma_{\alpha} + \Gamma_{\beta} + \Gamma_{\gamma})^2} \quad (4)$$

The model has been used previously to explain experimental findings of asymmetrical vibrational energy transfer,[44] as well as vibrational energy transfer in proteins.[45,46] A graphical representation of the three-mode processes is depicted in Figure 5.

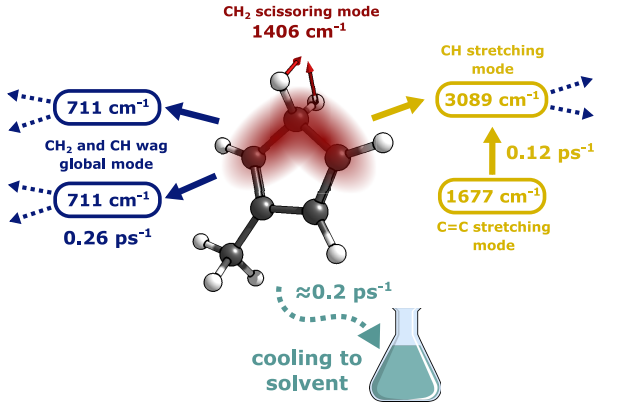

Figure 5. An example of two possible energy pathways leading from a vibrationally excited mode (red). On the left, in blue, the mode splits into two modes it is coupled with—corresponding to the "decay" process. On the right, in yellow, the mode "collides" with another populated mode, moving the energy upward.

The anharmonic constants $\Phi_{\alpha\beta\gamma}$ can be calculated using ab initio electronic structure methods readily available in several quantum chemistry packages as they are primarily used in the context of computational (infrared) spectroscopy. They also make up almost the entirety of the required resources for this step of the workflow, though in our case they are still more affordable than a single AIMD trajectory.

We obtained them using Gaussian's implementation of GVPT2,[47] which also includes the treatment of frequency shifts due to both anharmonicity and resonances of the vibrational states. This allows us to bypass the similarly formulated second set of self-consistent equations which would describe the frequency shifts[43] and therefore to focus only on the decay Γ.

Computational Details. All electronic structure calculations are performed using either the Gaussian 16[48] (geometries, GVPT2 frequencies, coupling constants, and forces) or ORCA 5[33] (transition state optimization with NEB-CI) software packages. AIMD trajectories were propagated using the Milo v1.1.0[49] dynamics program. Geometries in the figures were visualized with ChemCraft.

We showcase two levels of theory: a computationally less demanding DFT method in the form of the range-separated

https://doi.org/10.1021/acs.jctc.4c01011
J. Chem. Theory Comput. 2024, 20, 9048−9059

hybrid density functional CAM-B3YLP[50] with the def2-TZVP[51,52] basis set and D3BJ empirical dispersion,[53] a combination which should provide numerically stable anharmonic constants[54] and good value for computation time with medium-sized systems,[55] and second-order Møller–Plesset perturbation theory (MP2)[56] with the cc-pVTZ basis set[57] as our practical limit for obtaining anharmonic couplings. As previously discussed, we were limited to broken-symmetry unrestricted DFT calculations when obtaining the transition state and running AIMD simulations.

Insight into the accuracy of obtaining both frequency and coupling constants can be taken from benchmarks already present in the field of computational spectroscopy and examples, including the application of GVPT2, can be found in a recent review by Barone et al.[58] It is worth mentioning that the cost of the relatively expensive anharmonic calculation can be efficiently reduced via a hybrid approach—calculating harmonic frequencies at a higher level of theory and obtaining their anharmonic corrections with a more affordable approach. We have observed that the results depend much more on differences in computed vibrational frequencies as they may change the ordering of the modes and move them in or out of resonance. Their respective couplings, when strong enough to be significant, would stay large even at different levels of theory.

Since the decay rate depends on itself (Γ_α) as well as the decay rates of the other two modes (Γ_β, Γ_γ), this set of equations needs to be solved self-consistently. However, the dependence is small and it is also reasonable[44] to assume the Γ (in the right side of eq 3) add up to a line width of 24 cm^{-1}, putting the total Γ near the empirical value of 1 ps^{-1}, appropriate for organic molecules of this size. This effectively fixes the width of the Lorentzian curve that "searches" for resonances. By leaving a decent width available to each mode we will lose quantitative accuracy, but ensure we do not miss resonances due to the difficulties of calculating accurate vibrational frequencies.

The Master Equation. After obtaining the decay rates, we can then construct the matrix of transfer rates from one mode to another, **k**. In this work, we examine these transfer rates as a map of possible pathways for relaxation from one mode to another.

The **k** matrix is built up as shown in eq 5. The relaxation rate $\Gamma_{\alpha\beta}$ that makes up the off-diagonal elements is a subset of the sum of all terms from eqs 3 and 4, in which we take those terms that contain both the modes α and β. Additionally, the lifetime is obtained simply as the reciprocal value of the total decay rate of a vibrational mode, Γ_α.

$$k_{\alpha\beta} = \frac{\omega_\beta}{\omega_\alpha}\Gamma_{\alpha\beta}\, k_{\alpha\alpha} = -\left(\Gamma_{\alpha,\text{solvent}} + \sum_{\beta\neq\alpha} k_{\alpha\beta}\right) \tag{5}$$

Constant decay into the solvent is included in the diagonal elements at a value of $\Gamma_{\alpha,\text{solvent}} = 0.2\ ps^{-1}$. The results themselves are not very sensitive to this value, it simply ensures energy is removed from the system. However, a larger solvent decay will bring down the value of all estimated lifetimes. The resulting lifetime of 5 ps is the lower bound of values reported for molecules of similar size in organic solvents.[19,59]

The matrix **k** is used in a master equation approach to follow how a given energy distribution changes over time, with a simulation time step of 0.01 fs and the approximation noted in eq 6.

$$\mathbf{E}(t) = e^{\mathbf{k}t}\mathbf{E}_0 \approx (1 + \mathbf{k}t)\mathbf{E}_0 \tag{6}$$

Since the energy assigned to each mode changes over time we used occupation numbers n directly from our initial projected energies (as $n_\alpha = E_\alpha/\hbar\omega_\alpha$) and updated them every step for the first 1 ps of the simulation and every 20 steps afterward. Recomputing the **k** matrix adds cost while allowing for more collision pathways to be available. Since these are usually not the dominant ones, updating the **k** matrix less often yields very similar results.

We note that there may be interesting energy dynamics among some vibrational states that may not appear in the results of the master equation simulations. For example, energy may be trapped temporarily among a subset of modes and exhibit resonant oscillations, which the master equation would not predict. Nevertheless, bottlenecks to energy relaxation due to strong coupling among such modes and weak coupling to the others would be captured by the master equation approach, at least to the extent that the interactions among the modes are largely due to third-order anharmonic coupling.

Single-Valued Indicators. We will now expand the discussion to include the nonsubstituted **CP** ring structure explored in ref 31, as well as three other substituents: a methoxy group (**OMe**), chloromethyl group (**CH2Cl**) and tertbutyl group (**TB**). This provides us with examples of both different system sizes and vibrations of different character.

The final challenge of using this information to aid reaction design is the data analysis. Molecules have many vibrational modes that "talk to each other" and mapping them out visually becomes impossible. For example, any in-depth analysis will involve looking for major pathways for vibrational modes that either start with the most energy or point toward the rearranged product, as well as plotting the energy contained in certain fragments or bonds of the molecule.

This becomes a problem if we wish to quickly sample and compare the effects of changing the structure. Ideally, a single number indicator that quantifies how likely the molecule is to exhibit nonstatistical behavior would not only help explain current nonstatistical reactions but also aid in reaction discovery—which is currently dominated by either assumptions of statistical dynamics and barrier estimations or massive applications of ab initio molecular dynamics. For this purpose, we will attempt to devise an indicator that aims to show how quickly the initial excitation can relax. We formulate it as eq 7:

$$\text{Indicator} = \frac{\sum_i \frac{E_i}{\omega_i}\cdot\frac{1}{\Gamma_i}}{\sum_i \frac{E_i}{\omega_i}} \tag{7}$$

where E is the estimated initial energy of the mode (from any projection scheme), ω is its frequency (in matching energy units) and Γ is the calculated IVR rate. Simply put, we multiply the estimated initial energy in each mode by its lifetime according to the IVR model and normalize it by the total estimated quanta of excitation in the region/molecule. As the decay rate Γ includes the empirical solvent decay of 0.2 ps^{-1}, the maximum lifetime of any mode is capped at 5 ps, which in turn also ensures this indicator will always stay in a range between 0 and 5 ps.

If a reaction is exhibiting useful nonstatistical behavior due to energy localization, we would then aim for structural changes that increase this value (as close to the limit set by the solvent). On the other hand, if we wished to prevent nonstatistical effects, we would aim to add relaxation pathways

https://doi.org/10.1021/acs.jctc.4c01011
J. Chem. Theory Comput. 2024, 20, 9048−9059

and lower the value of this indicator. In essence, a low value represents well-damped modes that lead to statistical results, while those closer to the solvent limit are underdamped.

To extract more relevant information from the data, we may also choose to define a group of modes of interest or a group of atoms that make up the reaction center and compute the indicator and plot only for those modes. In this case, we will choose the CH_2 group along with its two neighboring carbon atoms (highlighted in Figure 6) as our reaction center and focus on only modes localized to that region (details of this assignment can be found in the SI). We will refer to the region as "**3C**".

A more biased approach, picking out modes that specifically position the ring for a hydrogen rearrangement, might be more fruitful, but this way we hope to include all of them without adding manual work to the workflow. As this specific reaction may involve some tunneling, it is also important to include all modes whose combined displacements help better position the CH_2 hydrogen atoms. Figure 7 shows which modes of **2-MeCP** fall into this grouping.

Finally, since propagating the master equation has negligible cost compared to our previous steps, we wish to extract information from the actual time evolution. The simplest way to do this (for any set of modes) is to determine the time when there is only $\frac{1}{e}$ (around 36.79%) of the initial energy remaining. As energy can flow both in and out of the chosen set, this value may go above 5 ps. The plots also provide a graphical way to interpret the results and we show some representative plots in Figure 8. The first four plots, grouped by mode frequency, clearly show the common "tiered" nature of IVR as most of the energy flow will occur by the decay mechanism toward lower frequency modes. When looking at custom regions of interest such as in (e) and (f), the intermediate or steady-state might or might not appear, depending on whether energy flows into the region.

RESULTS AND DISCUSSION

From the plots in Figure 8, we see that some systems have much larger energy estimations, for example, **MeCP** in (c) compared to **OMe** in (d), even though they are of similar size. This is mainly due to the trajectory not coming as close to the local minimum of the PES on its first pass into the well. We ran trajectories for 100 fs and the first pass would always occur within the first 50 fs, however, running for longer and picking the second or third "bounce" did not guarantee a relevant improvement.

The resulting overestimation is mainly reflected in the highest energy modes (such as C−H stretches), where even small displacements contribute a lot of additional energy and resemble the (dotted) estimation obtained straight from the transition state. However, in terms of the single-valued indicators, we did not notice a much larger standard deviation of the ensemble result nor a larger difference between the single trajectory result and the ensemble mean. The results should stay robust, as long as a criterion is present to reject trajectories that completely miss the minimum.

Moving on to the computed indicators shown in Figure 6, we see that the values obtained for the **3C** region (b) are similar compared to those for the whole molecule (a). As the regional indicator (b) contains fewer modes overall, the differences between similar systems are more pronounced. As expected, the overall values decrease as the system size

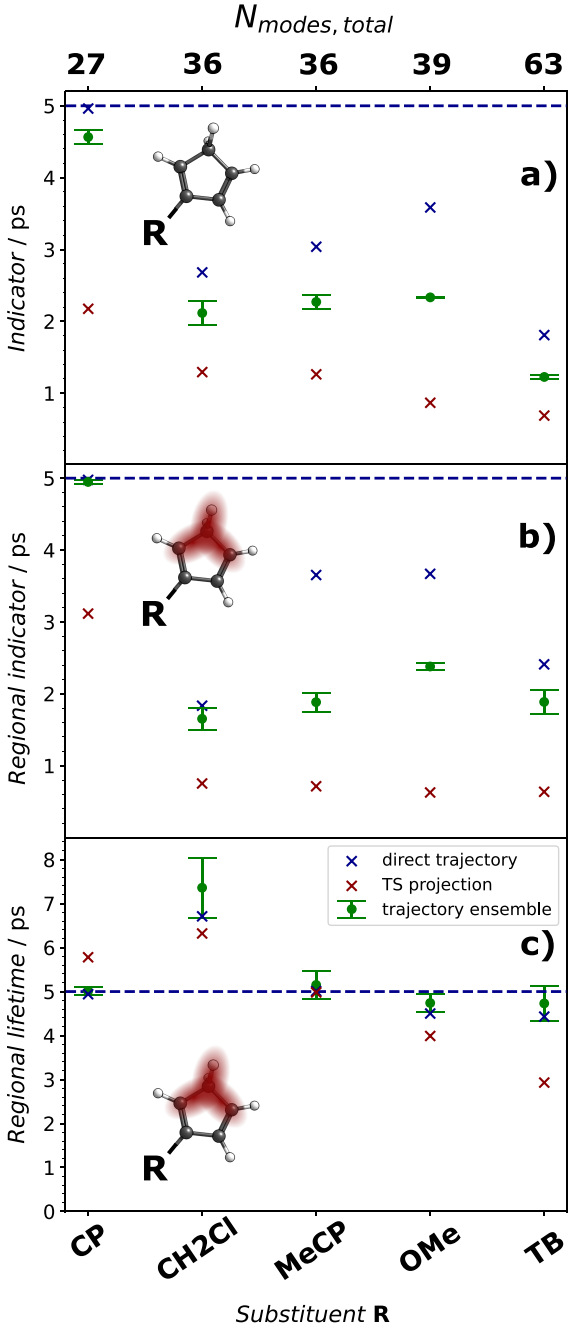

Figure 6. Indicator values for the relaxation of all modes (a) and those localized to the **3C** region (b) in differently substituted (R) systems; lifetimes computed from the master equation for the **3C** region modes (c). The dashed blue line represents the solvent decay limit to which all values would collapse with no intramolecular vibrational relaxation present. For each substituent change we use three different ways of estimating the initial excitation. The trajectory ensemble mean values (green circles) are capped above and below by their standard deviations.

increases and more relaxation pathways are added. There is, however, a clear dip in the three substituents (**CH2Cl**, **MeCP** and **OMe**) that are of similar size but different makeup, during which this trend actually reverses.

This is a typical example of how vibrational relaxation relies on a local density of states. Adding a substituent onto such a small ring creates many more pathways, but their effect is measured by how well they couple with existing ones. In the

https://doi.org/10.1021/acs.jctc.4c01011
J. Chem. Theory Comput. 2024, 20, 9048−9059

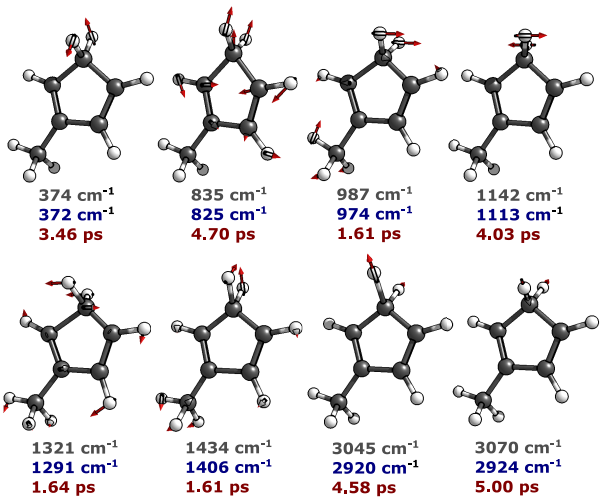

Figure 7. By defining the **3C** region using three carbon atoms and the two hydrogen atoms of the CH_2 group we focus on the vibrational relaxation of 8 out of a total of 36 vibrational modes in the example of **MeCP**. Modes obtained with DFT are shown here on displaced geometries (displacement scale of 0.5) with their scaled displacement vectors, harmonic frequency (gray), GVPT2 corrected frequency (blue), and computed relaxation lifetime (red). The computed lifetimes include the empirical solvent decay value and therefore have an upper bound of 5 ps.

extreme example of **TB** the system now has more than double the original number of modes. In the indicator value for the whole molecule (a) this large difference is still visible in the form of a second dip, but the "payoff" is less than switching out no substituent for a small one. For the values based on only the **3C** region of interest (b and c), **TB** is outcompeted by the heavy-atom effect in **CH2Cl**, as many of the modes added by the *tert*-butyl group are localized to its three branched methyl groups and simply too far away.

The dip at **CH2Cl** is also present in the computed lifetime of the **3C** region's modes (c), but in this case, it seems to point to the complete opposite of the indicator value. This can be explained by considering that the indicator values only describe the presence of usable vibrational relaxation pathways between the reaction center and the rest of the molecule. However, the lifetime value is computed directly from the master equation and as the coupling is present, energy can also flow into the region, depending on its initial distribution. In those cases, the lifetime can go above the imposed solvent relaxation limit of 5 ps.

For reference, the **3C** region contains 8 out of the total 36 modes in both the **MeCP** and **CH2Cl** systems (as shown in Figure 7). But changing one hydrogen to a chlorine atom more than triples the mass of the small substituent, changing some of the frequencies and couplings inside the ring itself and also how the system gains energy while dropping from the transition state. There are now 158 resonances that contribute more than 0.01 ps^{-1} to the total decay, an inclusion criterium we use to simplify and reduce noise, as opposed to 95 in **MeCP**. However, as the indicator estimates "first tier" relaxation and the **3C** modes do not change much, it only reports a slightly lower value. A good example is the highest frequency mode belonging to the **3C** region (the CH_2

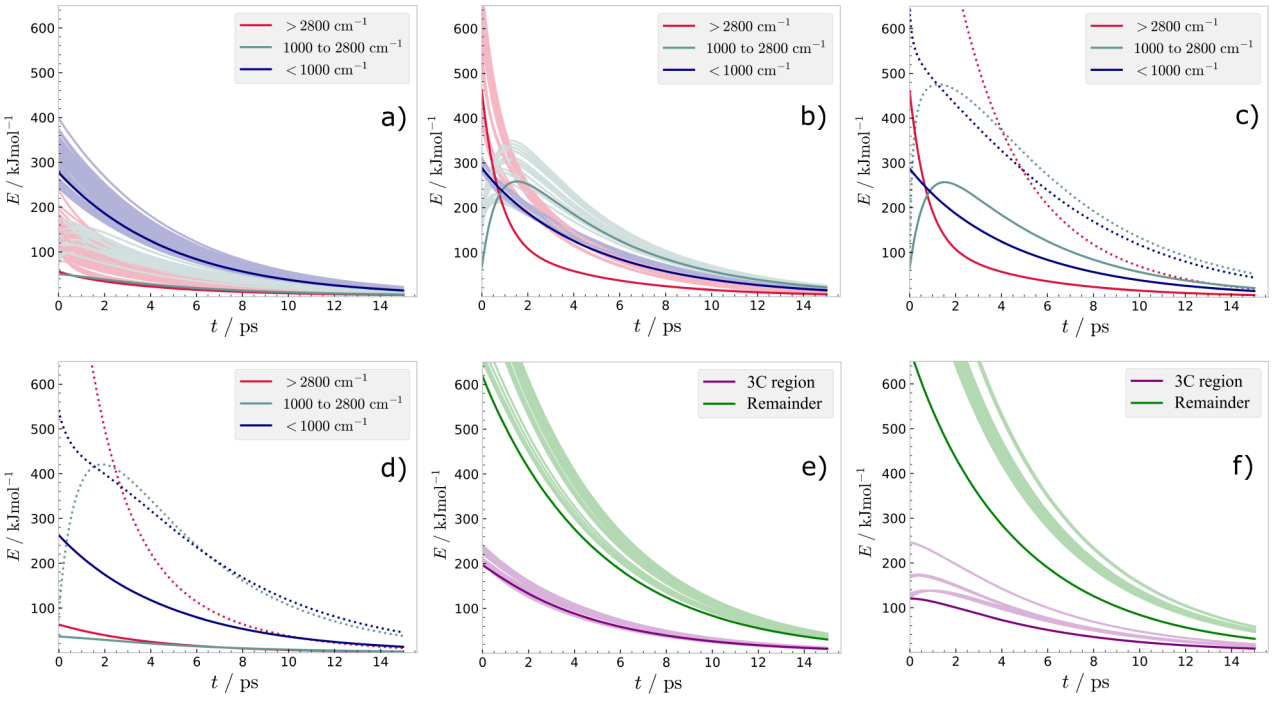

Figure 8. Model allows us to follow the energy in any group of vibrational modes, the obvious choices being groups by frequency range and those localized to a region/functional group of the molecule. While most of the IVR from the highest frequency modes (red) occurs very quickly, the tiered (bottlenecked) nature of IVR can lead to several time scales or steps being observed experimentally. The population of vibrations in the medium energy range (pastel green) peaks in the first few picoseconds, containing most of the "first tier" modes. We show (a) **CP** and (b) **MeCP** results from 50 trajectories (transparent) and from the single 0 K pushed trajectory (solid); followed by 0 K pushed trajectory results (solid line) compared to TS projection results (dotted) for (c) MeCP and (d) OMe. The last two plots show the time evolution by grouping the modes into two regions for (e) **MeCP** and (f) **CH2Cl**.

https://doi.org/10.1021/acs.jctc.4c01011
J. Chem. Theory Comput. 2024, 20, 9048−9059

Table 1. Computed BS-DFT Single-Point Energy (ΔE, in kJmol^{-1}) and Gibbs Energy (ΔG, in kJmol^{-1}) Differences for the First Barrier (TS, Reactant to Transition State) and the Drop towards the First Product (1-TS, Transition State to First Product) along with the Imaginary Frequency at the Transition State (ν_{TS}); in Vacuum and with Implicit Solvent Modeling for Tetrahydrofuran

substituent	ΔE_{TS}	ΔE_{1-TS}	ΔG_{1-TS}	ν_{TS}/cm^{-1}	$\Delta E_{TS,THF}$	$\Delta E_{1-TS,THF}$	$\Delta G_{1-TS,THF}$	$\nu_{TS,THF}$/cm^{-1}
CP	112.6	316.7	301.5	−688	44.5	250.5	235.8	−668
CH2Cl	113.8	314.1	301.0	−653	114.2	296.9	287.6	−641
MeCP	113.6	311.0	298.2	−659	113.4	312.1	299.4	−642
OMe	116.8	318.5	303.7	−637	117.8	318.3	303.7	−646
TB	115.0	308.4	295.1	−633	115.0	310.2	296.8	−636

asymmetric stretch at 2928 and 2924 cm^{-1} for CH2Cl and MeCP respectively), as it has no viable pathways of relaxation in either system.

Only by considering the master equation results of individual modes, we can see two representative modes that exhibited the longer lifetime steady state for **CH2Cl** - a symmetric global mode at 1377 cm^{-1} and a ring stretching mode at 826 cm^{-1} that resembles the ring-breaking mode of the TS. Interestingly, the frequencies of these vibrational modes are not changed, as they are 1379 and 825 cm^{-1} respectively in the **MeCP** system. However, they do rely on a small number of pathways created by the low-energy modes—which do change more, an example being the CH_2 (and ring) wagging mode at 384 cm^{-1} in **CH2Cl** that is very distorted compared to the same wagging motion in **MeCP** at 372 cm^{-1}, also resulting in a smaller coupling constant Φ for one of these pathways (decay: 1377 to 384 + 972 falling from 11.1 to 6.5 cm^{-1}). As many changes like this one can add up, it would be prudent not to skip the master equation, especially since running it is orders of magnitude faster than obtaining the couplings.

As all of the systems are still relatively small, we have effectively modulated the localization of energy by adding a heavy atom to the ring substituent. As a result, IVR of the reactive region in **CH2Cl** has actually slowed down, even though the overall density of states of the system increased. In a larger molecule, where we would imagine the majority of the energy moving away from the nonstatistical reaction center, we should see the indicators and lifetimes point in the same direction. This heavy atom effect is known from classic works by R. A. Marcus, William L. Hase, and co-workers. Inherently the effect is caused by frequency changes and mode localization, though a decrease in the number of useful resonances also makes IVR more sensitive to changes in couplings. For functional groups bridged by heavier atoms, a heavy atom blocking effect can arise and further isolate energy localization.[60,61]

As for excitation estimation, the single 0 K pushed trajectory method gives overall the same qualitative behavior and insight as the 50 trajectory ensemble. Since no zero-point energy is provided, the 0 K pushed trajectory results in a much more localized energy profile, resulting in higher indicator values (that is, less of the coupling reported as significant). The single-valued indicator results from a TS projection are not far from the dynamical picture from one or more trajectories, as the results depend on the common vibrational pathway structure. However, we risk losing any nuance between similar systems as we are essentially providing an excess of energy to the highest energy modes whose subsequent decay may mask any relevant energy localization in the midenergy or "tier two" modes. Overall, going down to a single trajectory approach will bring down the cost by one or 2 orders of magnitude, while choosing to use no AIMD at all would only halve it from there, as couplings are still required.

It is also worth noting that including anharmonic corrections for DFT frequencies does not always move them closer to experimental energy levels and resonances.[62] Since the GVPT2 calculation is costly and provides the resonance shift treatment, we prefer to use the provided anharmonic fundamentals in the model as well. For our results, switching back to harmonic frequencies does not change the results qualitatively (Figure S1), however for any larger exploration, we would advise checking benchmarks of the chosen electronic structure method.

On the other hand, MP2 results should generally benefit from GVPT2 corrections, but in our case, it would not be a reasonable choice of PES for the AIMD simulations. This led us to project coordinates and velocities from BS-DFT trajectories onto MP2 vibrational modes. Results from this mixing of methods are discussed in the Supporting Information. In short, the ordering of the substituents based on their calculated regional lifetime gives the same qualitative results. The indicator values differ, suggesting that they could be less robust metrics than directly obtained lifetimes, giving us another argument to propagate the master equation at little added expense.

Additionally, we performed implicit solvent calculations in tetrahydrofuran, as used in the experiment, for the single trajectory method, as well as the frequencies and couplings. With the unclear exception of the unsubstituted CP in solvent, barrier heights did not change much from substitution or solvation. An overview can be seen in Table 1. For CP, the first barrier is lower relative to both the CP and BCP structures, though it does not change the result obtained without solvation.

For all other systems, the differences in barrier heights are lower than the expected error of the energy projection scheme. The imaginary frequency at the top of the first barrier slightly decreases as the substituent size is increased. The results from implicit solvation, which are shown and discussed in the SI (Figure S1), qualitatively differ overall only in the regional indicator value.

It is important to note that in protic solvents a hydrogen-bonded solvent molecule could modify the vibrations of its bonded site, as well as draw some of the heat more efficiently. In those cases, one should consider including explicit solvent molecules in the electronic structure calculations and/or treat the bath (solvent) environment in a way where the cooling rates are not equal for all modes.

Additionally, coupling between vibrational and rotational (or torsional) motion may accelerate IVR, something that we do not capture with our current model. This is explained well in

https://doi.org/10.1021/acs.jctc.4c01011
J. Chem. Theory Comput. 2024, 20, 9048−9059

the work on the methyl rotor in *p*-fluorotoluene by Goodfellow and Parmenter,[63] where the increase in IVR (compared to difluoro benzene) is so large it cannot be justified by added modes and lowered symmetry alone. In our case, it is very likely the reported **MeCP** exhibits faster IVR, even if a purely vibrational model suggests it is similar to bulkier substituents.

Finally, we emphasize that these metrics aim to directly compare similar systems undergoing the same reaction mechanism. While we cannot propose direct product ratios, it is not guaranteed that a more exhaustive AIMD study would be able to either. In the previous study, only 2% of the BS-DFT trajectories at a sampling temperature of 1000 K were reactive, rising to 12% at 2000 K, while the experimental ratio of rearrangement was close to 20%.[31] But given this experimental data point for **MeCP** we can suggest that there are other substituents (such as CH_2Cl) where the rearrangement ratio would be higher. On the other hand, we would not expect a much smaller (more statistical) ratio despite switching out for a heteroatom group such as the methoxy, or a much larger tertbutyl group.

For completeness, in Scheme 2 we present a summary of the suggested procedure in which the steps match the proposed modeling scheme in Figure 2. Recently, GVPT2 anharmonic frequencies are also available in ORCA6, which we use alongside Gaussian16, though other quantum chemistry packages also offer the method. For dynamics, we provide a Jupyter notebook written for Milo, which is currently only interfaced with Gaussian, but which should be simple to adapt for other trajectories.

Scheme 2. A Summary of the Recommended Modeling Procedure

- **1a** Identify vibrationally hot intermediate/product and optimize its geometry with very tight convergence and SCF criteria
- **1b** Perform a GVPT2 calculation to obtain vibrational modes and their couplings and anharmonic frequencies
- **2a** (Optional) Obtain reaction path and TS guess using the NEB-CI method
- **2b** Optimize the geometry of the transition state preceding the hot intermediate/product
- **3** Start one or more molecular dynamics simulations at the TS geometry and run for 50-100 fs or stop automatically using criteria from Step 4
- **4** Project trajectory onto normal modes of intermediate/product and pick an appropriate point to estimate the vibrational excitation (implemented as Jupyter Python notebook)
- **5** Using the excitation estimate and GVPT2 output, run the IVR model (implemented in Python)
- **6a** Using plots and calculated lifetimes obtained from the IVR master equation, quantify the extent to which a certain set or region of vibrational modes is bottlenecked
- **6b** Use these insights to modify the structure to enhance or suppress non-statistical reactivity effects and repeat the procedure

In terms of improvements, the approach would overall benefit from a more accurate vibrational relaxation model, though its cost would need to be comparable. At present, we are looking into approximative methods of propagating quantum dynamics of the vibrational Hamiltonian. Approaches to performing semiclassical AIMD that reduce or remove zero-point energy leakage do exist and coupled with cost-efficient gradients could become viable for massed nonstatistical reaction exploration.

CONCLUSIONS

While AIMD simulations remain a popular tool for studying nonstatistical effects, computational and experimental techniques that quantify them are not in common use.[31] For this reason, we propose a combination of methods that estimate chemical excitation in terms of excess vibrational energy and then follow its (de)localization using an intramolecular vibrational relaxation model.

As the likelihood of nonstatistical chemical dynamics increases with greater energy localization, predicting the relaxation rates between reactive modes and the rest of the molecule sets us up to estimate the extent these effects could have on a chemical reaction. We achieve this by mapping out the restricted, tier-based energy transfer pathways.

This mode-centered approach has a clear relation to the molecular structure and remains less demanding than long time scale AIMD in terms of computational resources and postprocessing, though it lacks its exploratory nature for events occurring far away from the reference geometries. It is suitable for medium-sized organic molecules, but due to the local nature of these effects, structures that prove too large for anharmonic calculations can likely be cut down without loss of information.

In our example nonstatistical reaction we see that increasing system size does not guarantee either faster relaxation or less localization, and systems of identical size but distinct vibrational modes behave differently as new resonances emerge. Adding a tertbutyl substituent more than doubles the size of the base molecule, yet shows comparable results to the smaller substituents. From a reaction design standpoint, this suggests that the nonstatistical behavior could hold even as part of a much larger carbon backbone - while at the same time being sensitive to nearby heteroatoms.

In the future we aim to explore chemical systems of varying structure, using this model as a screening tool to guide chemical reactivity—by either introducing fragments that behave as nearby "heatsinks" or by breaking up existing, but unwanted, energy transfer pathways. The most significant predictions would then be tested in a synthetic lab. In this way, we hope to expand the applicability of this model from an analytical tool for difficult problems to a method of discovery for synthetic procedures in which the asymmetry of vibrational energy flow guides us toward a desired product.

ASSOCIATED CONTENT

Supporting Information

The Supporting Information is available free of charge at https://pubs.acs.org/doi/10.1021/acs.jctc.4c01011.

Python IVR model, MEP and transition state geometries, GVPT2 results, AIMD trajectories, and their vibrational analysis; and more detailed information on the region assignment and trajectory velocity decomposition schemes (PDF)

https://doi.org/10.1021/acs.jctc.4c01011
J. Chem. Theory Comput. 2024, 20, 9048−9059

AUTHOR INFORMATION

Corresponding Author

Gemma C. Solomon − *Nano-Science Center and Department of Chemistry and NNF Quantum Computing Programme, Niels Bohr Institute, University of Copenhagen, DK-2100 Copenhagen, Denmark;* orcid.org/0000-0002-2018-1529; Email: gsolomon@chem.ku.dk

Authors

Tomislav Rožić − *Nano-Science Center and Department of Chemistry, University of Copenhagen, DK-2100 Copenhagen, Denmark;* orcid.org/0000-0001-7591-1624

Matthew S. Teynor − *Nano-Science Center and Department of Chemistry and NNF Quantum Computing Programme, Niels Bohr Institute, University of Copenhagen, DK-2100 Copenhagen, Denmark;* orcid.org/0000-0002-6981-4809

Nađa Došlić − *Department of Physical Chemistry, Ruder Bošković Institute, HR-10000 Zagreb, Croatia;* orcid.org/0000-0001-6535-9020

David M. Leitner − *Department of Chemistry, University of Nevada, Reno, Nevada 89557, United States;* orcid.org/0000-0002-3105-818X

Complete contact information is available at: https://pubs.acs.org/10.1021/acs.jctc.4c01011

Notes

The authors declare no competing financial interest.

ACKNOWLEDGMENTS

We acknowledge Erona Shabani who visited our group and worked on applying this strategy to other reported non-statistical reactions. This project has received funding from the European Research Council (ERC) under the European Union's Horizon 2020 research and innovation programme (grant agreement No 865870). D.M.L. was supported by NSF grant CHE-2245240. N.D. acknowledges financial support from the Croatian Science Foundation (HRZZ grant no. HRZZ-IP-2022-10-4658).

REFERENCES

(1) Levine, I. N. *Physical Chemistry*, 6th ed.; McGraw-Hill, 2009.

(2) Shan, X.; Burd, T. A.; Clary, D. C. New Developments in Semiclassical Transition-State Theory. *J. Phys. Chem. A* **2019**, *123*, 4639−4657.

(3) Bao, J. L.; Truhlar, D. G. Variational transition state theory: theoretical framework and recent developments. *Chem. Soc. Rev.* **2017**, *46*, 7548−7596.

(4) Glowacki, D. R.; Harvey, J. N.; Mulholland, A. J. Taking Ockham's razor to enzyme dynamics and catalysis. *Nat. Chem.* **2012**, *4*, 169−176.

(5) Carpenter, B. K. Energy Disposition in Reactive Intermediates. *Chem. Rev.* **2013**, *113*, 7265−7286.

(6) Guo, H.; Liu, K. Control of chemical reactivity by transition-state and beyond. *Chemical Science* **2016**, *7*, 3992−4003.

(7) Lee, S.; Goodman, J. M. VRAI-selectivity: Calculation of selectivity beyond transition state theory. *Organic and Biomolecular Chemistry* **2021**, *19*, 3940−3947.

(8) Teynor, M. S.; Scott, W.; Ess, D. H. Catalysis with a Skip: Dynamically Coupled Addition, Proton Transfer, and Elimination during Au- and Pd-Catalyzed Diol Cyclizations. *ACS Catal.* **2021**, *11*, 10179−10189.

(9) Tantillo, D. J. *Beyond transition state theory—Non-statistical dynamic effects for organic reactions*; Academic Press Inc., 2021; Vol. *55*; pp. 1−16.

(10) Kabadi, V. N.; Rice, B. M. Molecular Dynamics Simulations of Normal Mode Vibrational Energy Transfer in Liquid Nitromethane. *J. Phys. Chem. A* **2004**, *108*, 532−540.

(11) Rice, S. A.; Dinner, A. R. *Advancing Theory for Kinetics and Dynamics of Complex, Many-Dimensional Systems: Clusters and Proteins*; Komatsuzaki, T.; Berry, R. S.; Leitner, D. M., Eds.; Advances in Chemical Physics; John Wiley & Sons, Inc.: Hoboken, NJ, USA, 2011; Vol. *145*.

(12) Lourderaj, U.; Park, K.; Hase, W. L. Classical trajectory simulations of post-transition state dynamics. *Int. Rev. Phys. Chem.* **2008**, *27*, 361−403.

(13) Rush, L. A.; Gallo, K. F.; Stumetz, K. S.; Rodríguez-Pérez, I. A.; Cremeens, M. E. Non-statistical dynamics for the allene oxide to cyclopropanone conversion. *J. Phys. Org. Chem.* **2022**, *35*, No. e4385.

(14) Oda, K.; Tsutsumi, T.; Keshavamurthy, S.; Furuya, K.; Armentrout, P. B.; Taketsugu, T. Dynamically Hidden Reaction Paths in the Reaction of CF_3^+ + CO. *ACS Physical Chemistry Au* **2022**, *2*, 388−398.

(15) Carpenter, B. K. Dynamic Matching: The Cause of Inversion of Configuration in the [1,3] Sigmatropic Migration? *J. Am. Chem. Soc.* **1995**, *117*, 6336−6344.

(16) Liu, Y.; Holm, S.; Meisner, J.; Jia, Y.; Wu, Q.; Woods, T. J.; Martinez, T. J.; Moore, J. S. Flyby reaction trajectories: Chemical dynamics under extrinsic force. *Science* **2021**, *373*, 208−212.

(17) Tantillo, D. J. Dynamic effects on organic reactivity—Pathways to (and from) discomfort. *J. Phys. Org. Chem.* **2021**, *34*, No. e4202.

(18) Pein, B. C.; Sun, Y.; Dlott, D. D. Controlling Vibrational Energy Flow in Liquid Alkylbenzenes. *J. Phys. Chem. B* **2013**, *117*, 10898−10904.

(19) Pein, B. C.; Dlott, D. D. Modifying Vibrational Energy Flow in Aromatic Molecules: Effects of Ortho Substitution. *J. Phys. Chem. A* **2014**, *118*, 965−973.

(20) Karmakar, S.; Keshavamurthy, S. Intramolecular vibrational energy redistribution and the quantum ergodicity transition: a phase space perspective. *Phys. Chem. Chem. Phys.* **2020**, *22*, 11139−11173.

(21) Leitner, D. M. Quantum ergodicity and energy flow in molecules. *Adv. Phys.* **2015**, *64*, 445−517.

(22) Kurouchi, H.; Sanctis, I. L. A.-D.; Singleton, D. A. Controlling Selectivity by Controlling Energy Partitioning in a Thermal Reaction in Solution. *J. Am. Chem. Soc.* **2016**, *138*, 14534−14537.

(23) Chen, Q.; Zhang, S.; Hu, X.; Xie, D.; Guo, H. Reaction Pathway Control via Reactant Vibrational Excitation and Impact on Product Vibrational Distributions: The O + HO2 → OH + O2 Atmospheric Reaction. *J. Phys. Chem. Lett.* **2022**, *13*, 1872−1878.

(24) Witte, T.; Hornung, T.; Windhorn, L.; Proch, D.; de Vivie-Riedle, R.; Motzkus, M.; Kompa, K. L. Controlling molecular ground-state dissociation by optimizing vibrational ladder climbing. *J. Chem. Phys.* **2003**, *118*, 2021−2024.

(25) Kohler, B.; Krause, J. L.; Raksi, F.; Wilson, K. R.; Yakovlev, V. V.; Whitnell, R. M.; Yan, Y. Controlling the Future of Matter. *Acc. Chem. Res.* **1995**, *28*, 133−140.

(26) Dunkelberger, A. D.; Simpkins, B. S.; Vurgaftman, I.; Owrutsky, J. C. Vibration-Cavity Polariton Chemistry and Dynamics. *Annu. Rev. Phys. Chem.* **2022**, *73*, 429−451.

(27) Xiong, W. Molecular Vibrational Polariton Dynamics: What Can Polaritons Do? *Acc. Chem. Res.* **2023**, *56*, 776−786.

(28) Flowers, M. C.; Frey, H. M. Hot molecule effects in the thermal isomerization of methylbicyclo[2.1.0]pent-2-enes. *J. Am. Chem. Soc.* **1972**, *94*, 8636−8637.

(29) Golden, D. M.; Brauman, J. I. Thermal unimolecular isomerization of bicyclo [2.1.0]pent-2-ene. *Trans. Faraday Soc.* **1969**, *65*, 464.

(30) Farneth, W. E.; D'Amore, M. B.; Brauman, J. I. The isomerization of bicyclo[2.1.0]pent-2-enes. *J. Am. Chem. Soc.* **1976**, *98*, 5546−5552.

(31) Goldman, L. M.; Glowacki, D. R.; Carpenter, B. K. Nonstatistical dynamics in unlikely places: [1,5] Hydrogen migration in chemically activated cyclopentadiene. *J. Am. Chem. Soc.* **2011**, *133*, 5312−5318.

(32) Ásgeirsson, V.; Birgisson, B. O.; Bjornsson, R.; Becker, U.; Neese, F.; Riplinger, C.; Jónsson, H. Nudged Elastic Band Method for Molecular Reactions Using Energy-Weighted Springs Combined with Eigenvector Following. *J. Chem. Theory Comput.* **2021**, *17*, 4929−4945.
(33) Neese, F. Software update: The ORCA program system—Version 5.0. *WIREs Comput. Mol. Sci.* **2022**, *12*, No. e1606.
(34) Isobe, H.; Takano, Y.; Kitagawa, Y.; Kawakami, T.; Yamanaka, S.; Yamaguchi, K.; Houk, K. N. Systematic Comparisons between Broken Symmetry and Symmetry-Adapted Approaches to Transition States by Chemical Indices: A Case Study of the Diels-Alder Reactions. *J. Phys. Chem. A* **2003**, *107*, 682−694.
(35) Balcioglu, N.; Özgür Özsar, A. Thermal conversion of 1,3-hexadien-5-yne to benzene: a revisited theoretical study. *Journal of Molecular Structure: THEOCHEM* **2004**, *677*, 125−132.
(36) Oviedo, M. B.; Ilawe, N. V.; Wong, B. M. Polarizabilities of π-Conjugated Chains Revisited: Improved Results from Broken-Symmetry Range-Separated DFT and New CCSD(T) Benchmarks. *J. Chem. Theory Comput.* **2016**, *12*, 3593−3602.
(37) Skraba-Joiner, S. L.; Johnson, R. P.; Agarwal, J. Dehydropericyclic Reactions: Symmetry-Controlled Routes to Strained Reactive Intermediates. *Journal of Organic Chemistry* **2015**, *80*, 11779−11787.
(38) Kedziora, G. S.; Barr, S. A.; Berry, R.; M?ller, J. C.; Breitzman, T. D. Bond breaking in stretched molecules: multi-reference methods versus density functional theory. *Theor. Chem. Acc.* **2016**, *135*, 79.
(39) Hamaguchi, M.; Nakaishi, M.; Nagai, T.; Nakamura, T.; Abe, M. Notable Effect of an Electron-Withdrawing Group at C3 on the Selective Formation of Alkylidenecyclobutanes in the Thermal Denitrogenation of 4-Spirocyclopropane-1-pyrazolines. Nonstatistical Dynamics Effects in the Denitrogenation Reactions. *J. Am. Chem. Soc.* **2007**, *129*, 12981−12988.
(40) Malrieu, J.-P.; Trinquier, G. A Recipe for Geometry Optimization of Diradicalar Singlet States from Broken-Symmetry Calculations. *J. Phys. Chem. A* **2012**, *116*, 8226−8237.
(41) Mališ, M.; Loquais, Y.; Gloaguen, E.; Jouvet, C.; Brenner, V.; Mons, M.; Ljubić, I.; Došlić, N. Non-radiative relaxation of UV photoexcited phenylalanine residues: probing the role of conical intersections by chemical substitution. *Phys. Chem. Chem. Phys.* **2014**, *16*, 2285.
(42) Barbara, P. F.; Meyer, T. J.; Ratner, M. A. Contemporary Issues in Electron Transfer Research. *J. Phys. Chem.* **1996**, *100*, 13148−13168.
(43) Kuzmin, M.; Letokhov, V.; Stuchebryukhov, A. Threshold energy dependence of the intramolecular vibrational relaxation rate tor an isolated polyatomic molecule. *Soviet Phys.—JETP* **1986**, *63*, 264−271.
(44) Leitner, D. M.; Pandey, H. D. Asymmetric energy flow in liquid alkylbenzenes: A computational study. *J. Chem. Phys.* **2015**, *143*, 144301.
(45) Yu, X.; Leitner, D. M. Vibrational energy transfer and heat conduction in a protein. *J. Phys. Chem. B* **2003**, *107*, 1698−1707.
(46) Cui, Q.; Bahar, I., Eds. *Normal Mode Analysis*; Chapman and Hall/CRC, 2005; Chapter 15−16.
(47) Barone, V. Vibrational zero-point energies and thermodynamic functions beyond the harmonic approximation. *J. Chem. Phys.* **2004**, *120*, 3059−3065.
(48) Frisch, M. J.; Trucks, G. W.; Schlegel, H. B.; Scuseria, G. E.; Robb, M. A.; Cheeseman, J. R.; Scalmani, G.; Barone, V.; Petersson, G. A.; Nakatsuji, H.; Li, X.; Caricato, M.; Marenich, A. V.; Bloino, J.; Janesko, B. G.; Gomperts, R.; Mennucci, B.; Hratchian, H. P.; Ortiz, J. V.; Izmaylov, A. F.; Sonnenberg, J. L.; Williams-Young, D.; Ding, F.; Lipparini, F.; Egidi, F.; Goings, J.; Peng, B.; Petrone, A.; Henderson, T.; Ranasinghe, D.; Zakrzewski, V. G.; Gao, J.; Rega, N.; Zheng, G.; Liang, W.; Hada, M.; Ehara, M.; Toyota, K.; Fukuda, R.; Hasegawa, J.; Ishida, M.; Nakajima, T.; Honda, Y.; Kitao, O.; Nakai, H.; Vreven, T.; Throssell, K.; Montgomery, J. A., Jr.; Peralta, J. E.; Ogliaro, F.; Bearpark, M. J.; Heyd, J. J.; Brothers, E. N.; Kudin, K. N.; Staroverov, V. N.; Keith, T. A.; Kobayashi, R.; Normand, J.; Raghavachari, K.; Rendell, A. P.; Burant, J. C.; Iyengar, S. S.; Tomasi, J.; Cossi, M.; Millam, J. M.; Klene, M.; Adamo, C.; Cammi, R.; Ochterski, J. W.; Martin, R. L.; Morokuma, K.; Farkas, O.; Foresman, J. B.; Fox, D. J. *Gaussian 16, Revision A.03*; Gaussian Inc.: Wallingford CT, 2016.
(49) Teynor, M. S.; Wohlgemuth, N.; Carlson, L.; Huang, J.; Pugh, S. L.; Grant, B. O.; Hamilton, R. S.; Carlsen, R.; Ess, D. H. *Milo, Revision 1.1.0*; Brigham Young University: Provo, UT, 2022.
(50) Yanai, T.; Tew, D. P.; Handy, N. C. A new hybrid exchange−correlation functional using the Coulomb-attenuating method (CAM-B3LYP). *Chem. Phys. Lett.* **2004**, *393*, 51−57.
(51) Weigend, F.; Ahlrichs, R. Balanced basis sets of split valence, triple zeta valence and quadruple zeta valence quality for H to Rn: Design and assessment of accuracy. *Phys. Chem. Chem. Phys.* **2005**, *7*, 3297.
(52) Weigend, F. Accurate Coulomb-fitting basis sets for H to Rn. *Phys. Chem. Chem. Phys.* **2006**, *8*, 1057.
(53) Grimme, S.; Antony, J.; Ehrlich, S.; Krieg, H. A consistent and accurate ab initio parametrization of density functional dispersion correction (DFT-D) for the 94 elements H-Pu. *J. Chem. Phys.* **2010**, *132*, 154104.
(54) Sitkiewicz, S. P.; Zaleśny, R.; Ramos-Cordoba, E.; Luis, J. M.; Matito, E. How Reliable Are Modern Density Functional Approximations to Simulate Vibrational Spectroscopies? *J. Phys. Chem. Lett.* **2022**, *13*, 5963−5968.
(55) Mitra, H.; Roy, T. K. Comprehensive Benchmark Results for the Accuracy of Basis Sets for Anharmonic Molecular Vibrations. *J. Phys. Chem. A* **2020**, *124*, 9203−9221.
(56) Head-Gordon, M.; Head-Gordon, T. Analytic MP2 frequencies without fifth-order storage. Theory and application to bifurcated hydrogen bonds in the water hexamer. *Chem. Phys. Lett.* **1994**, *220*, 122−128.
(57) Dunning, T. H. Gaussian basis sets for use in correlated molecular calculations. I. The atoms boron through neon and hydrogen. *J. Chem. Phys.* **1989**, *90*, 1007−1023.
(58) Barone, V.; Ceselin, G.; Fusè, M.; Tasinato, N. Accuracy Meets Interpretability for Computational Spectroscopy by Means of Hybrid and Double-Hybrid Functionals. *Front. Chem.* **2020**, *8*, No. 584203.
(59) Park, S.-M.; Nguyen, P. H.; Stock, G. Molecular dynamics simulation of cooling: Heat transfer from a photoexcited peptide to the solvent. *J. Chem. Phys.* **2009**, *131*, 184503.
(60) Stuchebrukhov, A. A.; Marcus, R. A. Theoretical study of intramolecular vibrational relaxation of acetylenic CH vibration for v = 1 and 2 in large polyatomic molecules (CX3)3YCCH, where X = H or D and Y = C or Si. *J. Chem. Phys.* **1993**, *98*, 6044−6061.
(61) Swamy, K. N.; Hase, W. L. The heavy-atom effect in intramolecular vibrational energy transfera). *J. Chem. Phys.* **1985**, *82*, 123−133.
(62) Nejad, A.; Meyer, E.; Suhm, M. A. Glycolic Acid as a Vibrational Anharmonicity Benchmark. *J. Phys. Chem. Lett.* **2020**, *11*, 5228−5233.
(63) Longfellow, R. J.; Parmenter, C. S. How a (nearly) free methyl rotor accelerates intramolecular vibration relaxation. Theory and Experiment. *Journal of the Chemical Society, Faraday Transactions* **1988**, *84*, 1499.

https://doi.org/10.1021/acs.jctc.4c01011
J. Chem. Theory Comput. 2024, 20, 9048−9059